JACS
JOURNAL OF THE AMERICAN CHEMICAL SOCIETY
Article
pubs.acs.org/JACS

Confinement of Iodine Molecules into Triple-Helical Chains within Robust Metal–Organic Frameworks

Xinran Zhang,[†] Ivan da Silva,[‡] Harry G. W. Godfrey,[†] Samantha K. Callear,[‡] Sergey A. Sapchenko,[†,§] Yongqiang Cheng,[∥] Inigo Vitórica-Yrezábal,[†] Mark D. Frogley,[⊥] Gianfelice Cinque,[⊥] Chiu C. Tang,[⊥] Carlotta Giacobbe,[#] Catherine Dejoie,[#] Svemir Rudić,[‡] Anibal J. Ramirez-Cuesta,[∥] Melissa A. Denecke,[†] Sihai Yang,*[,†] and Martin Schröder*[,†]

[†]School of Chemistry, University of Manchester, Manchester M13 9PL, U.K.
[‡]ISIS Facility, STFC Rutherford Appleton Laboratory, Chilton, Oxfordshire OX11 0QX, U.K.
[§]Nikolaev Institute of Inorganic Chemistry, Siberian Branch of the Russian Academy of Sciences, Novosibirsk 630090, Russia
[∥]The Chemical and Engineering Materials Division (CEMD), Neutron Sciences Directorate, Oak Ridge National Laboratory, Oak Ridge, Tennessee 37831, United States
[⊥]Diamond Light Source, Harwell Science Campus, Oxfordshire OX11 0DE, U.K.
[#]European Synchrotron Radiation Facility, Grenoble 38043, France

Supporting Information

ABSTRACT: During nuclear waste disposal process, radioactive iodine as a fission product can be released. The widespread implementation of sustainable nuclear energy thus requires the development of efficient iodine stores that have simultaneously high capacity, stability and more importantly, storage density (and hence minimized system volume). Here, we report high I_2 adsorption in a series of robust porous metal–organic materials, MFM-300(M) (M = Al, Sc, Fe, In). MFM-300(Sc) exhibits fully reversible I_2 uptake of 1.54 g g^{-1}, and its structure remains completely unperturbed upon inclusion/removal of I_2. Direct observation and quantification of the adsorption, binding domains and dynamics of guest I_2 molecules within these hosts have been achieved using XPS, TGA-MS, high resolution synchrotron X-ray diffraction, pair distribution function analysis, Raman, terahertz and neutron spectroscopy, coupled with density functional theory modeling. These complementary techniques reveal a comprehensive understanding of the host–I_2 and I_2–I_2 binding interactions at a molecular level. The initial binding site of I_2 in MFM-300(Sc), I_2^I, is located near the bridging hydroxyl group of the $[ScO_4(OH)_2]$ moiety [I_2^I···H–O = 2.263(9) Å] with an occupancy of 0.268. I_2^{II} is located interstitially between two phenyl rings of neighboring ligand molecules [I_2^{II}···phenyl ring = 3.378(9) and 4.228(5) Å]. I_2^{II} is 4.565(2) Å from the hydroxyl group with an occupancy of 0.208. Significantly, at high I_2 loading an unprecedented self-aggregation of I_2 molecules into triple-helical chains within the confined nanovoids has been observed at crystallographic resolution, leading to a highly efficient packing of I_2 molecules with an exceptional I_2 storage density of 3.08 g cm^{-3} in MFM-300(Sc).

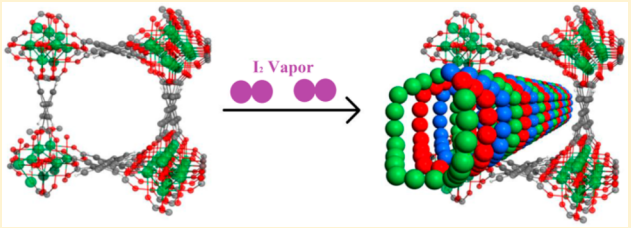

INTRODUCTION

Nuclear power supplied 11% of the electricity in the world in 2016.[1] Although it has ultrahigh energy density (500 million times higher than gasoline by volume), the widespread implementation of nuclear power has significant social effects and can be disastrous if not strictly and effectively controlled. In particular, iodine isotopes, if released as an airborne contaminant, can pose significant health risks to humans through the respiratory system via both beta and γ radiation.[2] Various capture systems, including zeolites,[3a,b] chalcogels,[3c] microporous polymers,[3d,e] porous aromatic frameworks,[3f] covalent[3g] or hydrogen-bonded[3h] organic frameworks have been tested for the removal of I_2. These systems, however, generally adopt irregular pore distributions, random adsorption sites and lack structural order, precluding the visualization of host–guest or guest–guest interactions.

Porous metal–organic frameworks (MOFs) are emerging hybrid solid adsorbents for a wide variety of gases,[4a] organic vapors,[4b] water[4c] and dyes.[4d] Constructed from metal ions bridged by organic ligands, MOFs often exhibit high porosity and tunable pore structures with desirable surface binding sites. Recently, the encapsulation of noble gases and heavy metal ions has been achieved in SBMOF-2[5a] and ZrDMBD,[5b] respectively, demonstrating the potential application of MOFs for the cleanup of nuclear wastes. More recently, adsorption of I_2 has been studied in a number of MOFs showing varying capacity,

Received: August 16, 2017
Published: October 11, 2017

DOI: 10.1021/jacs.7b08748
J. Am. Chem. Soc. 2017, 139, 16289–16296

reversibility and stability,[6] such as HKUST-1,[6a] ZIF-8,[6b] $[Zn_3(DL\text{-}lac)_2(pybz)_2]$ ($DL\text{-}lac^{2-}$ = lactate anion, $pybz^-$ = 4-pyridylbenzoate),[6c] [CuI(TMBP)],[6d] (TMBP = 3,3,5,5-tetramethyl-4,4-bipyrazole), and thiol-modified MIL-53(Al).[6e] To design future materials with improved I_2 adsorption, it is vital to understand the intermolecular contacts, location, and binding interactions of adsorbed guest molecules within the cavity of the host material. Determination of the binding of molecular I_2 within porous materials is a highly challenging task. First, adsorbed I_2 tends to have a high activation barrier for diffusion in the host structure (owing to its large molecular mass) resulting in high disorder within the pores of MOFs. Second, I_2 adsorption often induces severe structural disorder within the entire host−guest system; thus to date, determination of the locations of adsorbed I_2 molecules has only been achieved in exceptional cases, typically within MOF systems incorporating strongly hindered surface sites[6a,f] or geometrically confined pores[6b] in which the motion of adsorbed guest molecules is highly constrained. Thus, the nature of the host−I_2 and I_2−I_2 interaction(s) within MOF pores at a molecular level remains largely undefined.

Herein, we report the results of studies of adsorption of I_2 (up to 1.54 g g^{-1}) in a series of robust M(III)-tetracarboxylate materials, MFM-300(M) (M = Al, Sc, Fe, In) (MFM = Manchester Framework Material, replacing the NOTT designation).[7] Direct observation and quantification of adsorbed I_2 molecules within the MOF host have been achieved using a combination of high resolution synchrotron powder X-ray diffraction (PXRD), pair distribution function (PDF) analysis, Raman, Terahertz and neutron spectroscopy coupled with computational investigations. We found that at low loading the adsorbed I_2 molecules form specific interactions with metal-bound hydroxyl groups within the pore, supplemented by intermolecular interactions between adsorbed I_2 molecules. In contrast, at high loading, the intermolecular guest−guest interaction becomes the dominant feature and leads to an unusual self-aggregation of adsorbed I_2 molecules into ordered triple-helical chains within the confined channels. The cooperative interaction and formation of closely interacting triple-helical I_2 chains allow packing of I_2 molecules to an exceptional density of 3.08 g cm^{-3}, 63% of that for solid I_2 (4.93 g cm^{-3} at 298 K). Interestingly, to our best knowledge, the confined triple-helical iodine chains reported here are the first example of such systems reported within porous materials.

MATERIALS AND METHODS

Synthesis of MFM-300(M) (M= Al, Sc, Fe, In). MFM-300(M) (M = Al, Sc, In) were synthesized following previously reported methods,[7] and the synthesis of the new compound, MFM-300(Fe), is described here in detail. Biphenyl-3,3′,5,5′-tetracarboxylic acid (244 mg, 0.74 mmol) and $FeCl_3{\cdot}6H_2O$ (800 mg, 2.96 mmol) were dispersed in a mixture of DMF solution (20 mL) and concentrated hydrochloric acid (0.75 mL) in a 50 mL round-bottom flask under ambient pressure. The reaction was heated at 120 °C for 72 h. The yellow powder precipitate was collected and washed with DMF and acetone and then dried in air. Yield: 310 mg (89%). Elemental analysis: $[Fe_2(OH)_2(C_{16}H_6O_8)]{\cdot}(H_2O)_{1.5}{\cdot}(C_3H_7NO)_{1.8}$ (% calc/found) C 40.77/40.58 H 3.77/3.67 N 4.00/3.98. The acetone-exchanged samples were prepared by soaking the as-synthesized samples in an excess of acetone for 3 days with the acetone replaced every 12h. Elemental analysis $[Fe_2(OH)_2(C_{16}H_6O_8)]{\cdot}(H_2O)_{2.2}{\cdot}C_3H_6O$ (% calc/found) C 40.06/40.06, H 3.26/3.42, N 0/0. Selected IR(ATR): ν/cm^{-1} = 3448(br), 1700(s), 1609(s), 1526(s), 1455(s), 1421(s), 1373(s), 1315(s), 1095(s), 968(s), 783(s), 719(s), 708(s).

Characterization of Porosity. The acetone-exchanged MOF samples were dried in air and treated at 150 °C and 10^{-10} bar for 8 h to yield the fully desolvated samples, which were then loaded in a Tristar II PLUS (Micrometrics company) for porosity characterization. The BET surface areas and total pore volume were calculated using the N_2 isotherms measured at 77 K for MFM-300(Sc, In, Fe) or CO_2 isotherms measured at 273 K for MFM-300(Al).

Iodine Adsorption. Prior to adsorption, the acetone-exchanged samples were heated under dynamic vacuum (10^{-5} mbar) for 1 day at 150 °C. The activated sample was then transferred into a vessel, which contained a small amount of solid I_2 in an open vial and the vessel charged with dry N_2 at atmospheric pressure. The vessel was then sealed and heated at 80 °C for 0.5−20 h under N_2 to allow adsorption of I_2 into the desolvated MOFs. The I_2-loaded samples were cooled to room temperature and collected for further analysis.

Thermogravimetric−Mass Spectrometry (TGA-MS) Analysis. Thermogravimetric analysis (SDTQ600 TA Instruments company) combined with mass spectroscopy (Hiden DSMS analyzer) was used to determine the uptake of adsorbed I_2 molecules within MFM-300. Samples were heated from room temperature to 600 °C at a rate of 10 degree min^{-1} under a flow of air. The uptake of I_2 in MFM-300 was determined by the weight loss of adsorbed I_2 shown by the two characteristic peaks at 127 (I·) and 254 (I_2).

X-ray Photoelectron Spectroscopy. X-ray photoelectron spectroscopy (XPS) was carried out on an Axis Ultra DLD spectrometer (Kratos) using a monochromated Al Kα X-ray source (1486.6 eV, 13 mA, analysis area 300 × 700 μm). A charge neutralizer was used to compensate for any differential charging or any poor connection between the sample and sample plate (and thus ground). Survey spectra were collected with a pass energy of 80 eV and high-resolution core level spectra collected with a pass energy of 20 eV. Sample positions were optimized using fast acquisition of a narrow binding energy region, enabled by the delay line detector, of a pertinent photoelectron peak. The experiments were performed under ultrahigh vacuum conditions at pressures <3 × 10^{-8} mbar.

Pair Distribution Function (PDF) Analysis. PDF data were collected at beamline ID22 at the European Synchrotron Radiation Facility using a two-dimensional detector (PerkinElmer XRD 1611CP3) and an incident X-ray beam with λ = 0.19057 Å (Q_{max} = 24 $Å^{-1}$). The data were further processed with the help of GudrunX software[8a] and the computational analysis was achieved using the PDFGui software.[8b]

High Resolution X-ray Powder Diffraction Data. High resolution synchrotron X-ray powder diffraction (PXRD) data were collected at Beamline I11 of Diamond Light Source using multi-analyzing crystal-detectors (MACs) and monochromated radiation [λ = 0.827136(2)Å]. The powder samples were loaded into capillary tubes of 0.7 mm diameter and the data collection was carried out at room temperature.

Terahertz Spectroscopy. The THz spectra were measured with a liquid He cooled silicon bolometer detector from IR Laboratories at the MIRIAM beamline B22 of Diamond Light Source. The spectrometer was an in vacuum Bruker Vertex 80 V equipped with a beamsplitter in the FTIR of 6 μm thick multilayer mylar with a nominal transmission range from 600 to 100 cm^{-1}. Typically 512 scans were averaged per spectrum with an FTIR scanner velocity of 40 kHz at the reference laser wavenumber (15 799 cm^{-1}). The spectral resolution was 2 cm^{-1}.

Raman Spectroscopy. Raman spectra were obtained using an Xplora PLUS Raman microscope (Horiba Company) with a 785 nm laser and a 1200 lines/mm grating. The acquisition time was 10 s and accumulated for 5 cycles.

Inelastic Neutron Scattering (INS). INS experiments were undertaken at the beamline TOSCA at the ISIS Facility. The bare and I_2-loaded MFM-300(Sc) materials were loaded into two 11 mm diameter vanadium sample cans. The sample can was loaded into a closed cycle refrigerator (CCR) He cryostat and cooled to 11 K for data collection.

Structure Determination of MFM-300(Fe) and I_2-Loaded MFM-300(Sc). Rietveld refinements of PXRD data of the samples at

DOI: 10.1021/jacs.7b08748
J. Am. Chem. Soc. 2017, 139, 16289−16296

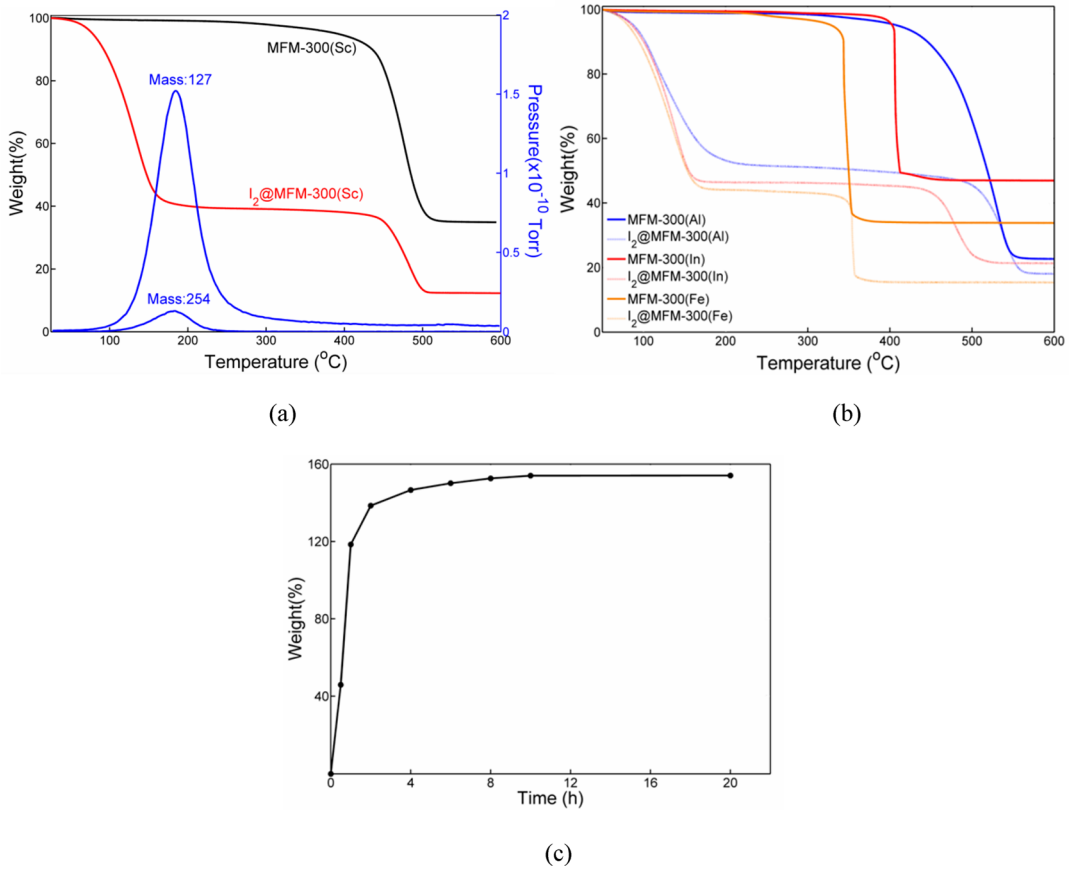

Figure 1. (a) TGA-MS data for bare and I_2-loaded MFM-300(Sc); (b) TGA plots and I_2 adsorption capacities of MFM-300(M) (M = Al, In, Fe). (c) Amount of I_2 adsorption in MFM-300(Sc) as a function of time.

various I_2 loadings were performed with Topas Academic 5 software package (Table S1). The structure of MFM-300(Fe) was determined by considering the structural model of MFM-300(Al).[7a] The crystallographic sites of adsorbed iodine atoms within MFM-300(Sc) were determined by electron density peak analysis of sequential difference Fourier maps. Positions of the metal and organic linkers of the framework were fixed during intermediate Rietveld refinements, but were included in the final refinement together with the positions of the iodine atoms. Final Rietveld refinements include lattice parameters, profile and background coefficients, all atomic positions and occupancies for iodine atoms (constrained to be the same value for the atoms within each I_2 molecule), and these yielded highly satisfactory agreement factors with an overall Rwp of around 6%.

Structure Determination of I_2-Loaded MFM-300(In). Single-crystal X-ray diffraction data of I_2-loaded MFM-300(In) were collected at 120 K using synchrotron radiation at Diamond Light Source Beamline I19 (Harwell Science and Innovation Campus, Didcot, UK) equipped with a three-circle goniometer and a Rigaku Saturn 724+ CCD detector (λ = 0.6889, double crystal monochromator with Si 111 cryo-cooled crystals). Data collection, frame integration and data reduction and processing were performed using DIALS.[9] Absorption correction was performed using the AIMLESS program.[10] The structures were solved by direct methods and refined on F^2 by full-matrix least-squares technique in the anisotropic approximation (for non-hydrogen atoms) using SHELX-2014.[11] Positions of hydrogen atoms on organic ligands and on the hydroxyl groups were calculated geometrically and refined in the riding model. The crystallographic data and details of the structure refinements are summarized in (Table S2). Selected interatomic distances are given in (Table S3).

DFT Calculations. Density function theory (DFT) calculations were performed using CASTEP.[12] The Generalized Gradient Approximation (GGA) as implemented by Perdew–Burke–Ernzerhof (PBE) was used to describe the exchange-correlation interactions. Norm-conserving pseudopotentials were employed to account for the effects of core electrons. The unit cell configurations determined by PXRD (Table S1) were used as the initial structure for the simulations. Atomic coordinates were relaxed to allow minimization of the potential energy and the interatomic forces. The energy tolerance for the electronic structure calculations was 5 × 10−10 eV, and the energy tolerance for ionic relaxation was 5 × 10^{-9} eV. The tolerance for the interatomic forces was 0.001 eV/Å. After convergence was reached, the dynamical matrix was obtained using the linear response method on a 1 × 1 × 2 gamma-centered mesh, from which the phonon frequencies and vibrational modes were calculated on a 3 × 3 × 3 gamma-centered mesh. The electronic structure calculations were performed on a 2 × 2 × 3 Monkhorst–Pack mesh. The O'Climax software[13] was used to convert the DFT-calculated phonon results to simulated INS spectra.

RESULTS AND DISCUSSION

Synthesis and Crystal Structure Analysis. The synthesis of the series of isostructural MOFs, MFM-300(M) (M = Al, Sc, In), was conducted following the reported methods.[7] The synthesis of MFM-300(Fe) is reported here for the first time. The solvated framework complex $[Fe_2(OH)_2(C_{16}H_6O_8)]\cdot(H_2O)_{1.5}\cdot(C_3H_7NO)_{1.8}$ was prepared via solvothermal reaction of H_4L (H_4L = biphenyl-3,3′,5,5′-tetracarboxylic acid) and $FeCl_3\cdot 6H_2O$ in dimethylformamide (DMF) and was isolated as a microcrystalline yellow powder. Structure solution by synchrotron powder X-ray diffraction confirmed that this material crystallizes in the tetragonal space group $I4_122$, and is isostructural to the related MFM-300(Al, Sc, In) materials.[7] MFM-300(Fe) exhibits an open structure consisting of chains of $[FeO_4(OH)_2]$ moieties bridged by tetracarboxylate ligands

DOI: 10.1021/jacs.7b08748
J. Am. Chem. Soc. 2017, 139, 16289–16296

Table 1. Summary of I_2 Adsorption Data in Selected MOFs[a]

MOFs	BET surface area (m^2/g)	pore size (Å)	pore volume ($cm^3\ g^{-1}$)	iodine uptake ($g\ g^{-1}$)	I_2 packing density ($g\ cm^{-3}$)
MFM-300(Sc)	1250	8.1	0.50	1.54	3.08
MFM-300(In)	1050	7.6	0.41	1.16	2.83
MFM-300(Fe)	1192	7.8	0.46	1.29	2.80
MFM-300(Al)	1370	6.5	0.37	0.94	2.54
Zn_3(DL-lac)$_2$(pybz)$_2$ [6c]	763	10.5	0.40	1.00	2.48
$Zr_6O_4(OH)_4(peb)_6$ [6h]	2650	14.2	1.16	2.79	2.41
HKUST-1 [6a]	1850	5.0−13.5	0.74	1.75	2.36
ZIF-8 [6b]	1630	3.4−11.6	0.66	1.25	1.89
$Zr_6O_4(OH)_4(sdc)_6$ [6h]	2900	11.9	1.33	1.07	0.80
Micro-Cu_4I_4-MOF [6i]	641	19 × 17	0.31	0.13	0.42

[a]H_2-DL-lac = DL-lactic acid. Hpybz = 4-pyridyl-benzoic acid. H_2peb = 4,4′-[1,4-phenylenebis(ethyne-2,1-diyl)]-dibenzoic acid. H_2sdc = 4,4′-stilbene-dibenzoic acid.

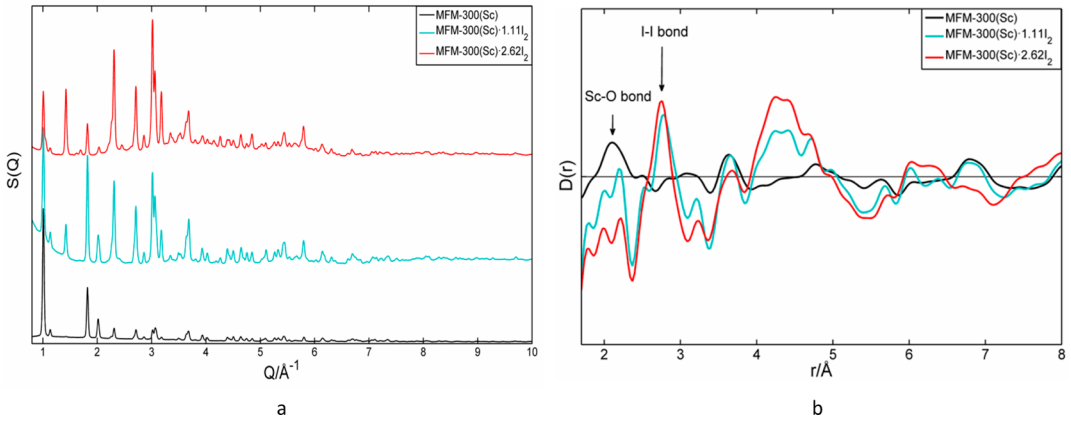

Figure 2. (a) Comparisons of diffraction patterns between bare MFM-300(Sc), MFM-300(Sc)·1.11I_2 and MFM-300(Sc)·2.62I_2. (b) Comparison of the PDF data for the bare MFM-300(Sc) and I_2-loaded MFM-300(Sc).

L^{4-} to afford a porous structure with channels formed by corner-sharing [$FeO_4(OH)_2$] octahedra linked via two mutually *cis*-μ_2-OH groups. The *cis*-μ_2-OH groups in MFM-300(Fe) tie the framework into a rigid "wine-rack" arrangement. Desolvated MFM-300(Fe) displays a surface area of 1193 $m^2\ g^{-1}$ (a total pore volume of 0.46 $cm^3\ g^{-1}$), as determined from the N_2 isotherm at 77 K, consistent with the porosity derived from the crystal structure (pore volume of 0.46 $cm^3\ g^{-1}$). The porosity data for MFM-300(M) (M = Al, Sc, In) materials are comparable to those previously reported, and confirm the complete activation and phase purity of these materials.

Studies of I_2 Adsorption in MFM-300. The complete activation of desolvated MFM-300 materials has been confirmed by the absence of weight loss up to 200 °C as determined by TGA (Figure 1). The adsorption of I_2 was conducted via diffusion of sublimated I_2 vapor into the desolvated MFM-300 materials at 70 °C under dry N_2. The samples undergo color changes upon adsorption of I_2 from white/pale yellow for the original samples to dark brown for I_2-loaded samples (Figure S1). Overall, the adsorption reached saturation after 10 h, and the maximum uptake of I_2 by MFM-300(M) was calculated by TGA-MS, to be 0.94, 1.54, 1.29, and 1.16 $g\ g^{-1}$ for M = Al, Sc, Fe, and In, respectively (Figure 1). The I_2 uptakes in MFM-300 are comparable to the well-behaved MOFs, such as HKUST-1 (1.75 $g\ g^{-1}$),[6a] $\{[(ZnI_2)_3(TPT)_2]\cdot 5.5(C_6H_5NO_2)\}_n$ [TPT = 2,4,6-tris(4-pyridyl)-1,3,5-triazine] (1.73 $g\ g^{-1}$),[6f] ZIF-8 (1.25 $g\ g^{-1}$),[6b] [$Ni(44pba)_2$] [44pba$^-$ = 4-(4-pyridyl)benzoate] (1.10 $g\ g^{-1}$).[6g] MFM-300(Sc) shows the highest I_2 uptake across the MFM-300 series and a more detailed study of I_2 uptake in MFM-300(Sc) was carried out as a function of time (t = 0.5−20 h) (Figure 1c). Between t = 0 to 2 h, there is increasing uptake of I_2 in MFM-300(Sc), and with time the rate of I_2 uptake reduces gradually to reach saturation after ca. t = 10 h.

The uptake of I_2 within all MFM-300 materials is reversible and the host can be fully regenerated upon desorption under heating. Based upon a pore filling model at saturation, the density of adsorbed I_2 in MFM-300 can be calculated using the pore volume and the saturated I_2 uptake and compared with a number of reported MOFs[6a−c,i,h] (Table 1). Interestingly, MFM-300 show very high storage densities (2.54−3.08 $g\ cm^{-3}$) of I_2 in the pore. Significantly, an exceptional density of 3.08 $g\ cm^{-3}$ has been obtained for adsorbed I_2 in MFM-300(Sc), exceeding those reported for the state-of-the-art MOFs such as [Zn_3(DL-lac)$_2$(pybz)$_2$] (2.48 $g\ cm^{-3}$), [$Zr_6O_4(OH)_4(peb)_6$] (peb^{2-} = 4,4′-[1,4-phenylenebis(ethyne-2,1-diyl)]-dibenzoate) (2.41 $g\ cm^{-3}$), HKUST-1 (2.36 $g\ cm^{-3}$) and ZIF-8 (1.89 $g\ cm^{-3}$) (Table 1). This value is 63% of that for solid I_2 (4.93 $g\ cm^{-3}$ at 298 K) and indicates highly efficient packing of adsorbed I_2 molecules within the pores of MFM-300(Sc).

Analysis of the XPS and SEM of MFM-300 upon Adsorption of I_2. X-ray photoelectron spectroscopy (XPS) was used to determine the valence of adsorbed I_2 in MFM-300(Sc) (Figure S9). The appearance of the single characteristic peak at 620.1 eV is indicative of only one type of adsorbed I_2 species in the pore and all adsorbed I_2 molecules remain neutral. In other words, there is little difference in the binding environment of the I_2 molecules in MFM-300(Sc). The

DOI: 10.1021/jacs.7b08748
J. Am. Chem. Soc. 2017, 139, 16289−16296

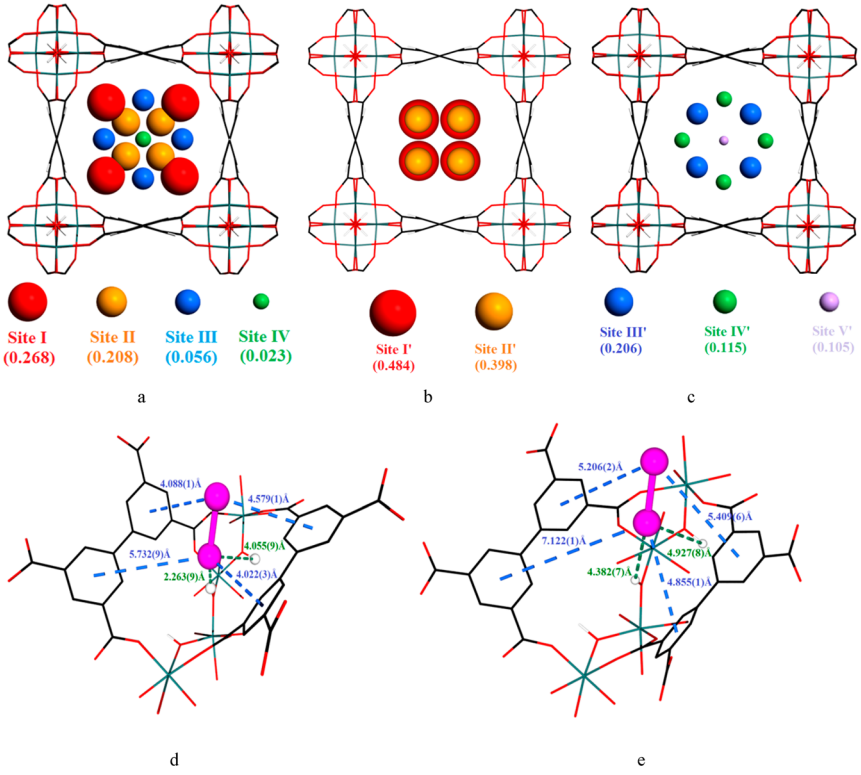

Figure 3. Views of the binding sites along the *c* axis for adsorbed I_2 molecules at different I_2-loadings: (a) MFM-300(Sc)·1.11I_2; (b) and (c) MFM-300(Sc)·2.62I_2. Views of the primary binding site in (d) MFM-300(Sc)·1.11I_2 and (e) MFM-300(Sc)·2.62I_2.

absence of morphological changes in the crystallites of MFM-300(Sc) upon adsorption of I_2 was confirmed by SEM (Figure S10), and EDX data showed homogeneous distribution of I_2 throughout MFM-300(Sc) and the absence of any bulk surface adsorbed I_2 (Figure S11).

PXRD and PDF Analysis of I_2-Loaded MFM-300(Sc). The stability and potential evolution in the host materials were monitored by PXRD as a function of I_2 loading. All MFM-300 samples showed similar trends by PXRD upon I_2 adsorption and the details for MFM-300(Sc) are described here. On increasing loading of I_2, MFM-300(Sc) gradually loses its Bragg intensity via increased diffuse scattering of I_2 (Figure 2a). At saturation, the total X-ray scattering of I_2-loaded MFM-300(Sc) is dominated by adsorbed I_2 molecules because of its greater scattering length than other framework atoms. This indicates that the adsorbed I_2 molecules in MFM-300 are disordered which results in diffuse X-ray scattering rather than Bragg diffraction. Upon desorption of all adsorbed I_2 molecules, the crystallinity and all Bragg peaks of the host MOFs are recovered with no difference observed in their peak widths or heights. This confirms the full reversibility of I_2 adsorption and desorption, and the high stability of the host MOF materials (Figure S7a,b). Additionally, the surface area of regenerated MFM-300(Sc) was determined as 1150 $m^2\ g^{-1}$, comparable to that (1250 $m^2\ g^{-1}$) of the as-synthesized MFM-300(Sc).

To gain in-depth understanding of the local structure of I_2-loaded MFM-300(Sc), a PDF analysis of the atomic distance distribution was undertaken using a hard synchrotron X-ray beam (λ = 0.19057 Å). The PDF plot for the bare MOF shows excellent agreement with the structural model for desolvated MFM-300(Sc) (Figure S8). Furthermore, as shown in Figure 2b, with loading of I_2, a new peak at ca. 2.7 Å develops, and this can be assigned to the intramolecular I−I distance for adsorbed I_2 molecules. With increasing I_2 loading, the intensity of the peaks at 2.1 Å (corresponding to the Sc−O distance) and 2.7 Å decrease and increase, respectively, consistent with the appearance of host−guest disorder upon I_2 adsorption. Furthermore, a marked increase in intensity at ca. 4−5 Å was observed for I_2-loaded MFM-300(Sc) due to the formation of intermolecular interactions between adsorbed I_2 molecules and host−guest interactions between adsorbed I_2 and the MOF interior. Interestingly, similar changes of the PDF plots (i.e., reduction of the peaks associated with atoms in the MOFs structure and appearance of new peaks at ca. 2.7 and 4.5 Å) have been observed in HKUST-1 upon adsorption of I_2.[6a]

Determination of the Binding Domains for Adsorbed I_2 in MFM-300. To determine the binding domains of adsorbed I_2 in MFM-300, high resolution synchrotron PXRD data have been collected for MFM-300(Sc) with moderate and high I_2 loadings (1.11 and 2.62 I_2/formula, respectively). The I_2-loaded samples were annealed at 70 °C for 3 days prior to the data collection to ensure full diffusion of I_2 into and within the channels and to reduce structural disorder. Fourier difference map analysis of the PXRD data for the desolvated MOF indicates no residual electron density peak within the pore, thus confirming the complete activation and structural stability of the desolvated host. Comparison of the PXRD patterns for the bare and I_2-loaded samples revealed large variations in peak intensities and absence of new peaks, demonstrating the retention of host structure and adsorption of I_2 within the pore (Figure S13). Sequential Fourier difference map analysis of the PXRD patterns revealed the position of the adsorbed I_2 molecules, which was further developed by Rietveld refinement of these data.

For MFM-300(Sc)·1.11I_2, four independent binding sites (I, II, III and IV) are located within the 1D channel of MFM-

DOI: 10.1021/jacs.7b08748
J. Am. Chem. Soc. 2017, 139, 16289−16296

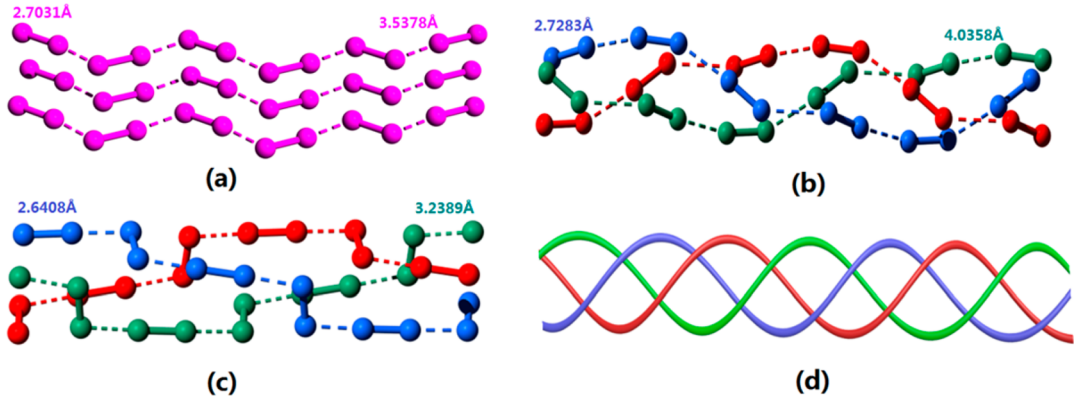

Figure 4. (a) View along the *a* axis of the crystal structure of I_2 in the solid state at room temperature; (b) views of the triple-helical chains of I_2 molecules inside MFM-300(Sc) and (c) MFM-300(In). (d) Schematic view of the assembly of triple-helical chains of iodine molecules.

300(Sc) (Figure 3). The major binding site I_2^I is located near the bridging hydroxyl group of the $[ScO_4(OH)_2]$ moiety [I_2^I···H−O = 2.263(9) Å] with an occupancy of 0.268. I_2^{II} is located interstitially between two phenyl rings of neighboring ligand molecules [I_2^{II}···phenyl ring = 3.378(9) and 4.228(5) Å], 4.565(2) Å from the hydroxyl group, with an occupancy of 0.208. The intermolecular distance between I_2^I and I_2^{II} is 2.827(2)Å. Sites III and IV reside in the middle of the pore, stabilized by intermolecular interaction and adopt low occupancies.

On additional I_2 loading for MFM-300(Sc)·2.62I_2 the adsorbed I_2 molecules in the pore of MFM-300(Sc) undergo notable rearrangement. Overall, the intramolecular interactions between I_2 molecules dominate over interactions between I_2 molecules and the surface binding sites of the framework. Five distinct binding sites (I′, II′, III′, IV′ and V′) have been identified for adsorbed I_2 molecules. Site I′ (occupancy = 0.484) lies between two phenyl rings [$I_2^{I'}$···ring centroid = 4.855(1)Å] and shows much weaker interaction with the bridging hydroxyl [$I_2^{I'}$···H−O = 4.382(7)Å] compared to that in MFM-300(Sc)·1.11I_2. Sites II′ and III′ (occupancy = 0.398 and 0.206, respectively) both form a weak hydrogen bond with the −OH moiety with distances of 3.827(6) and 4.475(8) Å, respectively. Sites IV′ and V′ (occupancy = 0.115 and 0.105, respectively) reside interstitially between sites I′, II′ and III′ via formation of guest−guest interactions, the binding distances of which (2.64−2.73 Å for intramolecular I−I; 3.24−4.04 Å for intermolecular I···I, subject to the site occupancy) are comparable to those observed in solid crystalline iodine (2.70 Å I−I; 3.54 Å I···I) (Figure 4).[10] The crystal structure has also been determined for MFM-300(Fe)·1.11I_2 by the PXRD method, and similar binding domains for adsorbed I_2 molecules as for MFM-300(Sc)·1.11I_2 have been observed (Figure S16−S17). The binding domain for adsorbed I_2 molecules within MFM-300(In) has also been determined by single crystal diffraction and a similar confinement of I_2 molecules into triple-helical chains was observed (Figure 4c and Table S2).

The intermolecular interaction between adsorbed I_2 molecules affords a self-aggregation mechanism to form highly unusual triple-helical chains running through the pore along the *c*-axis. The supramolecular assembly of these chains is stabilized by intermolecular dispersion forces at distances of ca. 4 Å. Interestingly, the formation of molecular chains of I_2 in confined nanospace as quantum objects has been reported in a theoretical study,[14a] which confirms the possible existence of single, double and triple helical chains of I_2 but predicts that a 4-fold chain will collapse entirely. To date, the formation of triple-helical chains of I_2 has only been observed once in single-walled carbon nanotubes studied by TEM at nanometer resolution.[14c] Additionally, the formation of one-fold linear polyiodide and zigzag chains of I_5^- and I_7^- has been observed in the channel of MOFs.[14d,e] In contrast, the formation of triple-helical chains of I_2 has been unambiguously observed in MFM-300(Sc) at crystallographic resolution and represents the first example of such a motif in porous MOFs.

Vibrational Analysis of the I_2-Loaded MFM-300(Sc) by INS/Far-IR/Raman Spectroscopy. Comparison of the Raman spectra of bare and I_2-loaded MFM-300(Sc) confirms the absence of change of local vibrational modes associated with the MOF structure (Figure 5a). At the low energy region, two types of adsorbed I_2 were observed. The peak at 180 cm^{-1} (regarded as I−I vibration)[15] is assigned to I_2 sited in the middle of the pores, with a frequency comparable to solid I_2. The peak at 170 cm^{-1} suggests the presence of adsorbed I_2 bound to the framework, and its small red-shift (Δ = 10 cm^{-1}) is attributed to the formation of hydrogen bonds between I_2 molecules and the hydroxyl bridges, entirely consistent with the above structural models. One might expect the interaction between the I_2 and the metal-hydroxyl groups to induce a partial dipole moment for these adsorbed I_2 molecules. Terahertz spectra, however, indicate an absence of I−I vibration (Figure 5b), suggesting that the weak binding interaction between the I_2 molecules and the MOF host is not sufficient to distort the symmetry of I_2 molecules, consistent with the supramolecular, reversible binding of I_2 molecules in MFM-300. Two peaks at 252 and 280 cm^{-1} (both assigned to the lattice vibrational modes via DFT modeling) disappear upon I_2 loading, consistent with the formation of closely packed I_2 molecules in the pore.

A combination of INS and DFT was applied to study the changes in the lattice and local modes within the MOF structure (Figure 6), particularly those involved in the formation of host−guest hydrogen bonds. Upon loading of I_2, a reduction in the scattering intensity in the low energy region (<30 meV) was observed, suggesting a stiffening of the host−guest system. Furthermore, the peaks at 114 and 117 meV (assigned as combinations of C−H and O−H bending modes) decrease in intensity upon I_2 loading, confirming the interaction of these groups with adsorbed I_2. The difference INS spectra (loaded minus bare MOF signal) clearly show these changes and are in excellent agreement with the DFT

DOI: 10.1021/jacs.7b08748
J. Am. Chem. Soc. 2017, 139, 16289−16296

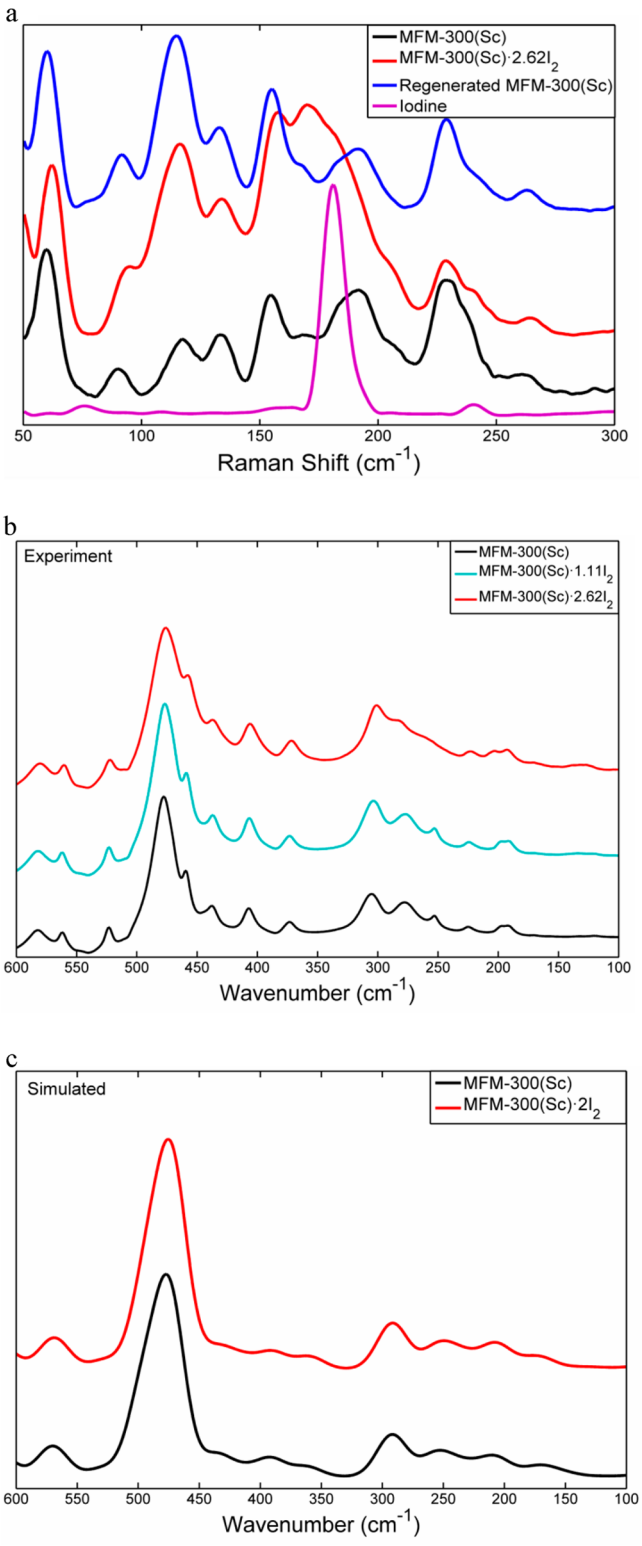

Figure 5. (a) Comparison of Raman spectra of bare MFM-300(Sc), MFM-300(Sc)·2.62I_2, regenerated MFM-300(Sc) and solid I_2 in the low energy region. Full spectra are shown in Figure S12. (b) Comparison of the terahertz spectra of bare MFM-300(Sc), MFM-300(Sc)·1.11I_2 and MFM-300(Sc)·2.62I_2. (c) Calculated DFT terahertz spectra of bare MFM-300(Sc) and MFM-300(Sc)·2I_2 (scale factor = 0.94 was used).

calculated spectra, further confirming the observed host–guest interactions in the structural models described above.

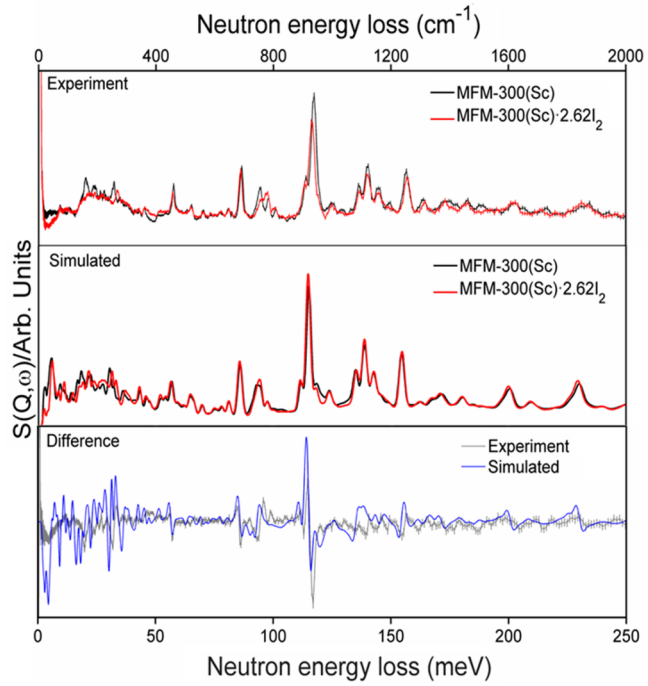

Figure 6. Comparison of the INS spectra of bare MFM-300(Sc) and MFM-300(Sc)·2.62I_2. Top: Experimental INS data. Middle: DFT-Calculated INS spectra. Bottom: Comparison of the experimental and calculated difference INS spectra, showing excellent agreement between the two.

Introduction of desirable functional groups and open metal sites into the pore structure has been widely regarded as an effective design of new MOFs to encapsulate I_2. For example in ZIF-8, the adsorbed I_2 molecules have been found to bind strongly within the small cage (~3.4 Å) containing methyl groups.[6b] Within HKUST-1, the primary binding site for adsorbed I_2 was located at near the Cu(II)-paddlewheels.[6a] Recently, the binding of adsorbed I_2 via $(I_4)^{2-}$ bridges has been reported in $\{[(ZnI_2)_3\text{-}(TPT)_2]\cdot 5.5(C_6H_5NO_2)\}_n$.[6f] Our study confirms that a combination of suitable pore size (6–8 Å) and shape/geometry (squared-shaped pore in this case) of channels and suitable pore decorations (e.g., hydroxyl groups) can provide a unique platform to stabilize the formation of a complex assembly of molecular I_2 resulting in highly efficient packing and hence the exceptional storage density of I_2.

CONCLUSIONS

In summary, we report the adsorption of large amounts of I_2 in a series of ultrastable MOF materials with excellent reversibility and full stability of the host materials. Several key insights into the binding of I_2 within the hydroxy-decorated material MFM-300(Sc) have been revealed multiple techniques. These observations have implications for the design and discovery of future materials capable of storing I_2 efficiently. The binding of I_2 within MFM-300 is mediated by a combination of weak intermolecular interactions at low loadings and strong guest–guest interactions at high loadings. More importantly, we report the experimental observation of the self-aggregation of I_2 within confined space, and the formation of a highly unusual triple-helical chain of I_2. An exceptional storage density of adsorbed I_2 in MFM-300(Sc) has been observed, and the adsorption and binding modes of I_2 within these materials have been rationalized by both experimental and theoretical investigations.

DOI: 10.1021/jacs.7b08748
J. Am. Chem. Soc. 2017, 139, 16289–16296

The strategy of confinement of I_2 within optimized pore environments is applicable to the capture and separation of radioactive iodine.

■ ASSOCIATED CONTENT

Supporting Information

The Supporting Information is available free of charge on the ACS Publications website at DOI: 10.1021/jacs.7b08748.

Synthetic details, experimental methods, details of X-ray and PDF refinements, SEM, Raman spectra and additional views of I_2 binding sites (PDF)

■ AUTHOR INFORMATION

Corresponding Authors

*sihai.yang@manchester.ac.uk
*m.schroder@manchester.ac.uk

ORCID

Martin Schröder: 0000-0001-6992-0700

Notes

The authors declare no competing financial interest.

CCDC 1558478−1558482 contain the supplementary crystallographic data for this paper. These data can be obtained free of charge from the Cambridge Crystallographic Data Centre via www.ccdc.cam.ac.uk/data_request/cif.

■ ACKNOWLEDGMENTS

M.S. thanks the ERC for an Advanced Grant (AdG 226593), EPSRC (EP/I011870) and the University of Manchester for funding, and acknowledges the Russian Ministry of Science and Education for the award of a Russian Megagrant (14.Z50.31.0006). We are especially grateful to STFC for access to TOSCA, to Oak Ridge National Laboratory (ORNL) for access to the Beamline VISION, to Diamond Light Source for access to Beamlines I11(EE14341) and B22(SM14938) and to the European Synchrotron Radiation Facility (ESRF) for access to Beamline ID22. The computing resources were made available through the VirtuES and ICEMAN projects, funded by Laboratory Directed Research and Development program at ORNL. X.R. Zhang acknowledges financial support from Chinese Scholarship Council for providing the studentship. S.A.S. thanks the Russian Science Foundation for the financial support (Grant 17-73-10254).

■ REFERENCES

(1) World Nuclear Association Home Page. http://www.world-nuclear.org (accessed Jul 1, 2017).

(2) Weber, W. J.; Roberts, F. P. *Nucl. Technol.* **1983**, *60*, 178.

(3) (a) Sakurai, T.; Izumo, M.; Takahashi, A.; Komaki, Y. *J. Nucl. Sci. Technol.* **1983**, *20*, 784. (b) Pham, T. C. T.; Docao, S.; Hwang, I. C.; Song, M. K.; Choi, D. Y.; Moon, D.; Oleynikov, P.; Yoon, K. B. *Energy Environ. Sci.* **2016**, *9*, 1050. (c) Subrahmanyam, K. S.; Malliakas, C. D.; Sarma, D.; Armatas, G. S.; Wu, J.; Kanatzidis, M. G. *J. Am. Chem. Soc.* **2015**, *137*, 13943. (d) Geng, T.; Zhu, Z. M.; Zhang, W.; Wang, Y. *J. Mater. Chem. A* **2017**, *5*, 7612. (e) Qian, X.; Zhu, Z. Q.; Sun, H. X.; Ren, F.; Mu, P.; Liang, W.; Chen, L.; Li, A. *ACS Appl. Mater. Interfaces* **2016**, *8*, 21063. (f) Yan, Z.; Yuan, Y.; Tian, Y.; Zhang, D.; Zhu, G. *Angew. Chem., Int. Ed.* **2015**, *54*, 12733. (g) Yin, Z. J.; Xu, S.; Zhan, T. G.; Qi, Q. Y.; Wu, Z. Q.; Zhao, X. *Chem. Commun.* **2017**, *53*, 7266. (h) Lin, Y.; Jiang, X.; Kim, S. T.; Alahakoon, S. B.; Hou, X.; Zhang, Z.; Thompson, C. M.; Smaldone, R. A.; Ke, C. *J. Am. Chem. Soc.* **2017**, *139*, 7172.

(4) (a) Yu, J.; Xie, L. H.; Li, J. R.; Ma, Y.; Seminario, J. M.; Balbuena, P. B. *Chem. Rev.* **2017**, *117*, 9674. (b) Decoste, J. B.; Peterson, G. W. *Chem. Rev.* **2014**, *114*, 5695. (c) Cadiau, A.; Belmabkhout, Y.; Adil, K.; Bhatt, P. M.; Pillai, R. S.; Shkurenko, A.; Martineau, C.; Maurin, G.; Eddaoudi, M. *Science* **2017**, *735*, 731. (d) Li, P.; Vermeulen, N. A.; Gong, X.; Malliakas, C. D.; Stoddart, J. F.; Hupp, J. T.; Farha, O. K. *Angew. Chem., Int. Ed.* **2016**, *55*, 1.

(5) (a) Chen, X.; Plonka, A. M.; Banerjee, D.; Krishna, R.; Schaef, H. T.; Ghose, S.; Thallapally, P. K.; Parise, J. B. *J. Am. Chem. Soc.* **2015**, *137*, 7007. (b) Yee, K. K.; Reimer, N.; Liu, J.; Cheng, S. Y.; Yiu, S. M.; Weber, J.; Stock, N.; Xu, Z. T. *J. Am. Chem. Soc.* **2013**, *135*, 7795.

(6) (a) Sava, D. F.; Chapman, K. W.; Rodriguez, M. A.; Greathouse, J. A.; Crozier, P. S.; Zhao, H.; Chupas, P. J.; Nenoff, T. M. *Chem. Mater.* **2013**, *25*, 2591. (b) Sava, D. F.; Rodriguez, M. A.; Chapman, K. W.; Chupas, P. J.; Greathouse, J. A.; Crozier, P. S.; Nenoff, T. M. *J. Am. Chem. Soc.* **2011**, *133*, 12398. (c) Zeng, M. H.; Wang, Q. X.; Tan, Y. X.; Hu, S.; Zhao, H. X.; Long, L. S.; Kurmoo, M. *J. Am. Chem. Soc.* **2010**, *132*, 2561. (d) He, J.; Duan, J.; Shi, H.; Huang, J.; Huang, J.; Yu, L.; Zeller, M.; Hunter, A. D.; Xu, Z. T. *Inorg. Chem.* **2014**, *53*, 6837. (e) Munn, A. S.; Millange, F.; Frigoli, M.; Guillou, N.; Falaise, C.; Stevenson, V.; Volkringer, C.; Loiseau, T.; Cibin, G.; Walton, R. I. *CrystEngComm* **2016**, *18*, 8108. (f) Brunet, G.; Safin, D. A.; Aghaji, M. Z.; Robeyns, K.; Korobkov, I.; Woo, T. K.; Murugesu, M. *Chem. Sci.* **2017**, *8*, 3171. (g) Mehlana, G.; Ramon, G.; Bourne, S. A. *Microporous Mesoporous Mater.* **2016**, *231*, 21. (h) Marshall, R. J.; Griffin, S. L.; Wilson, C.; Forgan, R. S. *Chem. - Eur. J.* **2016**, *22*, 4870. (i) Zhu, N. X.; Zhao, C. W.; Wang, J. C.; Li, Y. A.; Dong, Y. B. *Chem. Commun.* **2016**, *52*, 12702.

(7) (a) Yang, S.; Sun, J.; Ramirez-Cuesta, A. J.; Callear, S. K.; David, W. I. F.; Anderson, D. P.; Newby, R.; Blake, A. J.; Parker, J. E.; Tang, C. C.; Schröder, M. *Nat. Chem.* **2012**, *4*, 887. (b) Qian, J.; Jiang, F.; Yuan, D.; Wu, M.; Zhang, S.; Zhang, L.; Hong, M. *Chem. Commun.* **2012**, *48*, 9696. (c) Ibarra, I. A.; Yang, S.; Lin, X.; Blake, A. J.; Rizkallah, P. J.; Nowell, H.; Allan, D. R.; Champness, N. R.; Hubberstey, P.; Schröder, M. *Chem. Commun.* **2011**, *47*, 8304.

(8) (a) Soper, A. K.; Howells, S.; Hannon, A. C. ATLAS: Analysis of Time-of-Flight Diffraction Data from Liquid and Amorphous Samples; RAL Report RAL-89-046; Rutherford Appleton Laboratory: Chilton, Didcot, Oxon, U.K., 1999. (b) Farrow, C. L.; Juhas, P.; Liu, J. W.; Bryndin, D.; Božin, E. S.; Bloch, J.; Proffen, T.; Billinge, S. J. L. *J. Phys.: Condens. Matter* **2007**, *19*, 335219.

(9) (a) Waterman, D. G.; Winter, G.; Gildea, R. J.; Parkhurst, J. M.; Brewster, A. S.; Sauter, N. K.; Evans, G. *Acta Crystallogr., Sect. D Struct. Biol.* **2016**, *D72*, 558. (b) Evans, P. *Acta Crystallogr., Sect. D: Biol. Crystallogr.* **2006**, *D62*, 72.

(10) Evans, P. R.; Murshudov, P. R. *Acta Crystallogr., Sect. D: Biol. Crystallogr.* **2013**, *D69*, 1195.

(11) Sheldrick, G. M. *Acta Crystallogr., Sect. A* **2008**, *A64*, 112.

(12) Clark, S. J.; Segall, M. D.; Pickard, C. J.; Hasnip, P. J.; Probert, M. J.; Refson, K.; Payne, M. C. *Z. Kristallogr. - Cryst. Mater.* **2005**, *220*, 567.

(13) Ramirez-Cuesta, A. J. *Comput. Phys. Commun.* **2004**, *157*, 226.

(14) (a) Yao, Z.; Liu, C.; Li, Y.; Jing, X.; Yuan, Q. *Can. J. Phys.* **2017**, *7*, 1. (b) Fan, X.; Dickey, E.; Eklund, P.; Williams, K.; Grigorian, L.; Buczko, R.; Pantelides, S.; Pennycook, S. *Phys. Rev. Lett.* **2000**, *84*, 4621. (c) Guan, L.; Suenaga, K.; Shi, Z.; Gu, Z.; Iijima, S. *Nano Lett.* **2007**, *7*, 1532. (d) Yin, Z.; Wang, Q. X.; Zeng, M. H. *J. Am. Chem. Soc.* **2012**, *134*, 4857. (e) Hu, X. L.; Sun, C. Y.; Qin, C.; Wang, X. L.; Wang, H. N.; Zhou, E. L.; Li, W. E.; Su, Z. M. *Chem. Commun.* **2013**, *49*, 3564.

(15) Svensson, P. H.; Kloo, L. *Chem. Rev.* **2003**, *103*, 5.

DOI: 10.1021/jacs.7b08748
J. Am. Chem. Soc. 2017, 139, 16289−16296